Synthesis and luminescence properties of Tb^{3+} activated $CaO-Al_2O_3-B_2O_3$ glass

XIA WAN, QUAN ZHONG, SHAO-LONG TIE*, JUN-YIN SHEN
School of Chemistry and Environment, South China Normal University, Guangzhou 510006, PR China

A new high calcium aluminoborate glass with a simple composition of $CaO-Al_2O_3-B_2O_3$ (CaAlB) was synthesized and investigated detailedly by XRD, FT-IR, UV, DSC, and PL analysis methods. The results showed that this kind of glass matrix has a good thermal stability, fine transmittance in visible light, low absorption in VU wavelength, and fine ability of molten rare earth oxide. The luminescence of Tb^{3+}-doped glass phase showed the excitation peaks centred at 378 nm and 486 nm are assigned to the transitions of $^7F_6\rightarrow(^5D_3,^5G_6)$ and $^7F_6\rightarrow{}^6D_4$ of Tb^{3+}, respectively. The optimum doping concentration for Tb^{3+} was determined to be 15.6 mol% when excited by 378 nm, and the luminescence of Tb^{3+} straight increase with the Tb^{3+} concentration up to 21.9 mol% without concentration quenching when excited by 486 nm. The CIE chromatic coordinates, dominant wavelengths, and color purity values of Tb^{3+}-doped glasses were determined. The effects of Si^{4+} and Li^+ doping on the emission intensities of Tb^{3+} were investigated. Due to this Tb^{3+}-doped calcium aluminoborate glass can be excited by both ultraviolet and blue light, it may be an excellent luminescence material for LED.

(Received April 6, 2011; accepted May 31, 2011)

Keywords: Calcium aluminoborate glass, Tb^{3+} ion, Photoluminescence, CIE chromatic coordinate

1. Introduction

The luminescence properties of Tb^{3+} in glass matrix were investigated proverbially for recent years. The reported familiar glass matrixes contained silicate [1], borosilicate [2,3], borate [4,5], aluminosilicate [6,7], aluminoborate [8,9], sol–gel glasses [10,11], germanate [12], fluoride [13], and phosphate [14] et al. In a general way, silicate glasses have been extensively investigated since they possess stronger luminescence [15,16]. Borate glass is a suitable optical material with easily-shape and low melting temperature, but the "borate anomaly" in thermal expansion coefficient [17] became a problem. Among the glass components, Al_2O_3 has received consideration due to its high solubility for rare earth ions [18]. However, only a few studies were concerned about aluminoborate glass matrix. The luminescence properties of glass with the composition of $SrO-Al_2O_3-B_2O_3$ as Eu^{2+} and Dy^{3+} co-doped were studied by Huang et al. [8]. Krol et al. [9] reported that quantum yields of green (Tb^{3+}) emission under 254 nm wavelength excitation with the glass composition of $MO\cdot Al_2O_3\cdot B_2O_3\cdot Tb_2O_3$ (M = Mg, Ca, Sr, Ba and Zn) reached as high as 80%, but this kind of glass cannot been excited by light emitting diode (LED) chip. The glass with the composition of $BaO-Al_2O_3-B_2O_3$ was researched principally as encapsulation material for solid oxide fuel cell (SOFC) [19], vacuum technique and technology of electronics. However there is a lack of literature on the luminescence properties of dopants (rare earth ions) in aluminoborate glass system.

In this work, the high calcium aluminoborate glass with simple composition of $CaO-Al_2O_3-B_2O_3$ is taken into consideration as matrix in which rare earth ions (Tb^{3+}) are doped and a series of Tb^{3+}-doped calcium aluminoborate glasses were prepared. The properties of glass matrix were investigated by XRD, FT-IR, UV, DSC, and PL analysis methods. The photoluminescence emission and excitation behaviours of different Tb^{3+}-doped glasses have been analysed and the optimum concentrations were achieved under ultraviolet-light (378 nm) and blue-light (486 nm) wavelengths excitation.

2. Experimental methods

The glass samples were prepared from the mixtures of analytical reagents $CaCO_3$, $Al(OH)_3$, H_3BO_3, and high purity Tb_4O_7 (99.99%). These raw materials were ground equably, loaded into corundum crucible, placed into furnace and heated in advance at 1000 ℃ for 4 h, finally melted at 1200 ℃ for 3 h in air. Then, the melts were poured rapidly into a preheated stainless steel mold for cooling. The resultant glasses were annealed at 500 ℃ for 3 h to release inner stress. In all investigated glass samples, the doped ions were considered to replace Ca^{2+} ions in glass CaAlB in molar ratio. The prepared glasses $Ca_{1-x}AlB:Tb^{3+}{}_x$ with Tb^{3+} ions in a varied concentrations in the range of x = 0.0313, 0.0625, 0.0938, 0.125, 0.156, 0.188, and 0.219 mol have been considered to investigate concentration effect on its luminescence properties.

Comparatively, the series glasses components were in the range of (18%～40%) CaO, (17%～23%) Al_2O_3, (29%～38%) B_2O_3 and (0%～36%) Tb_2O_3 in mass percentage.

The powder X-ray diffraction analysis was carried out on a Beijing Puxi Y-2000 diffractometer to confirm the vitreous nature of glass powder. The FT-IR absorption spectrum was obtained from Hitachi IR-prespige-21 spectrometer with KBr pellet of glass powder. The UV-Vis absorption spectrum was measured with a Shimadzu UV-2550 spectrometer. The DSC curve of glass powder was obtained by Netzsch STA-409PC instrument with a programmed heating rate of 10 ℃/min in N_2 flow. The photoluminescence (PL) spectra were recorded on a Hitachi F-4500 spectrofluoremeter at room temperature with a xenon lamp.

3. Results and discussion

3.1 The structure of glass CaAlB

The XRD patterns of the glass matrix (CaAlB) powder (curve a) and Tb^{3+}-doped glass (curve b) are shown in Fig. 1. It is clear that both glass matrix and Tb^{3+}-doped glass reveal the broad bands with the center at 29.4^0 of two theta without specific patterns, confirming the vitreous nature of the prepared samples [7,20]. There is no change on the half-width of the broad band with Tb^{3+}-doped glass, indicating the stability of glass structure.

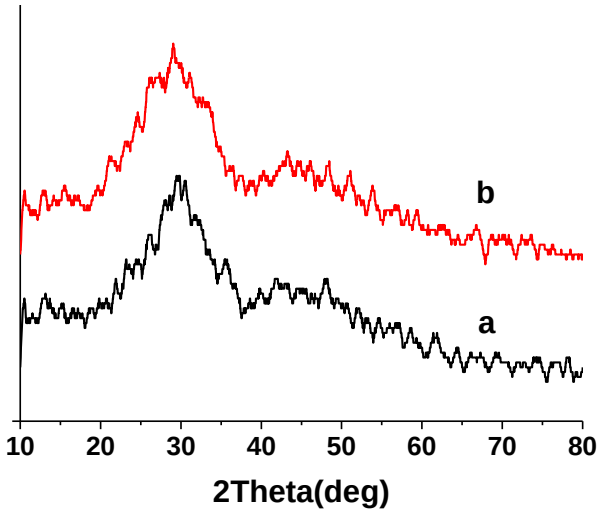

Fig. 1. The XRD patterns of glass CaAlB (a) and Tb^{3+}-doped glass CaAlB:Tb^{3+} (b).

Fig. 2 represents the FT-IR absorption spectrum of glass matrix powder. The strong absorption bands covering from 1450 cm^{-1} to 1200 cm^{-1} and around 875 cm^{-1} are due to the asymmetry and symmetry stretching vibration modes of B–O bond in [BO_3] structural unit, respectively [21]. The band around 715 cm^{-1} is attributed to the symmetric stretching vibration mode of Al-O band in [AlO_4] unit [22] or the bending vibration mode of B–O bond in [BO_3] unit [23]. The absorption band at 491 cm^{-1} is attributed to bending vibration mode of Al-O band in [AlO_4] unit [24]. The weak adsorption at 1023 cm^{-1} is due to the discriminative stretching vibration of reverse symmetry for [BO_4] unit [7,22]. When Al_2O_3 becomes part of glass composition, Al^{3+} ions snatch oxygen atoms from CaO and [BO_4], become [AlO_4] unit, induce the abatement of [BO_4] unit and the increase of [BO_3] unit [25]. Consequently, the prepared glass with the composition of CaO-Al_2O_3-B_2O_3 has a network building up with a mass of [BO_3] and [AlO_4] structural units and a few of [BO_4] units. This result is in accord with V. P. Klyuev's work [26].

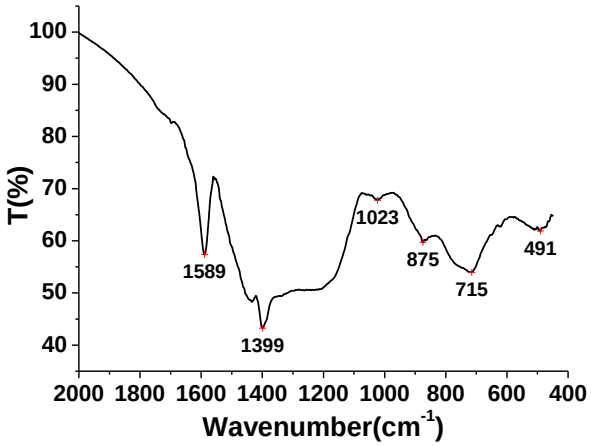

Fig. 2. The FT-IR spectrum of glass CaAlB powder.

The DSC curve of glass matrix powder was showed in Fig. 3. It be investigated that a glass transition temperature (T_g) appears at 632 ℃ [26], crystallization temperature (T_c) at 824 ℃, two exothermal crystallized temperature at 844 ℃ and 972 ℃, respectively, and melting temperature (T_m) at 995 ℃. These results confirm the facts that the glass with composition of CaO-Al_2O_3-B_2O_3 has high T_g temperature and large temperature interval ΔT (=T_c-T_g), indicating its good thermal stability and the fine ability against crystallization of glass.

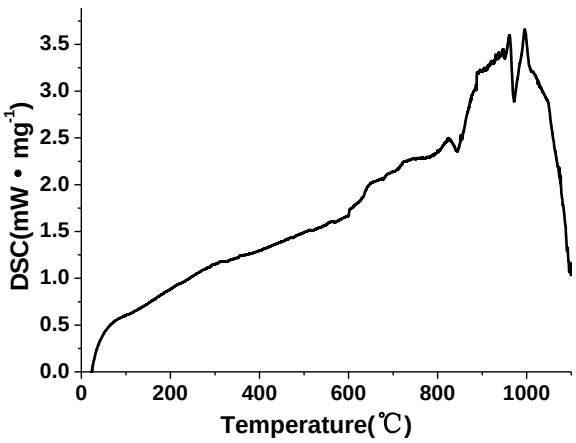

Fig. 3. The DSC curve of glass CaAlB powder.

3.2 Optical properties of glass CaAlB:Tb^{3+}

The UV-Vis absorption spectra of glass matrix (curve a) and Tb^{3+}-doped glass (curve b) were shown in Fig. 4. In glass matrix (curve a), there is almost no absorption from 300 nm to 900 nm wavelengths and small absorption between 200 nm and 300 nm wavelengths. In curve b, the UV–Vis absorption peaks centred at 485, 378, 368, 351, 337, and 317 nm assigned to the transitions from ground state $^7F_6$ to higher excited states of $^5D_4$, ($^5D_3$, $^5G_6$), $^5L_{10}$, ($^5L_9$, $^5G_4$), ($^5G_2$, $^5L_6$), and ($^5H_7$, $^5D_{0,\ 1}$) of Tb^{3+} ion, respectively, and the absorption band from 230 nm to 310 nm is due to the $4f^8 \rightarrow 4f^7 5d^1$ transition of Tb^{3+} [2,7]. These absorption bands can be also observed clearly from its excitation spectrum in Fig. 5.

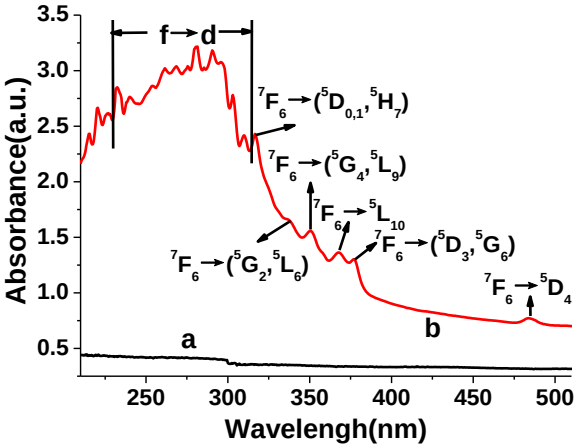

Fig. 4. The UV-Vis absorption spectra of glass CaAlB matrix (curve a) and Tb^{3+} doped glass (curve b).

Fig. 5 shows the excitation spectrum of Tb^{3+}-doped glass with composition of $Ca_{1\text{-}0.0625}AlB:Tb^{3+}{}_{0.0625}$ (0.0625 is relative molarity for Ca^{2+}) by monitoring at 544 nm wavelength. The excitation spectrum is composed of sharp bands in the range from 310 nm to 510 nm standing for $4f^8$–$4f^8$ transitions of the Tb^{3+} ions and a broad band from 220 nm to 310 nm comprising of $4f^8 \rightarrow 4f^7 5d^1$ transitions. The sharp bands in UV wavelength region (310 nm～400 nm) are located at 378, 369, 352, 340, and 317 nm, attributing to the Tb^{3+} transitions of $^7F_6 \rightarrow (^5D_3, ^5G_6)$, $^7F_6 \rightarrow ^5L_{10}$, $^7F_6 \rightarrow (^5L_9, ^5G_4)$, $^7F_6 \rightarrow (^5G_2, ^5L_6)$ and $^7F_6 \rightarrow (^5H_7, ^5D_{0,1})$, respectively; and in blue-light wavelength region (460 nm～510 nm) the excitation band centred at 486 nm is assigned to the Tb^{3+} transition of $^7F_6 \rightarrow ^5D_4$ [27,28]. All these excitation transitions are analogous to foregoing results in optical absorption spectrum (Fig. 4).

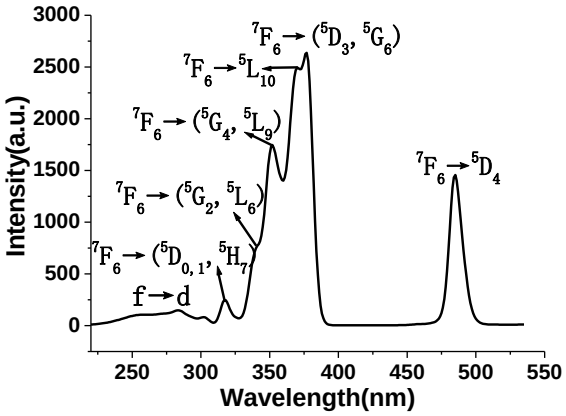

Fig. 5. The excitation spectrum of glass $Ca_{1\text{-}0.0625}AlB:Tb^{3+}{}_{0.0625}$ for 544 nm emission.

Fig. 6 shows the emission spectrum of Tb^{3+}-doped glass with composition of $Ca_{1\text{-}0.0625}AlB:Tb^{3+}{}_{0.0625}$ under 378 nm excitation. It is clear that those peaks locating at 488, 544, 585, and 622 nm are ascribed to $^5D_4 \rightarrow ^7F_{6,5,4,3}$ transitions, and several very weak peaks locating at 414, 436, and 457 nm (amplificatory drawing at the upper left) are attributed to $^5D_3 \rightarrow ^7F_{5,4,3}$ transitions [7]. The $^5D_4 \rightarrow ^7F_5$ transition (544 nm) obeys the selection rule of a magnetic dipole (MD) transition with $\triangle J = \pm 1$, showing a bright green luminescent color from Tb^{3+}-doped glasses.

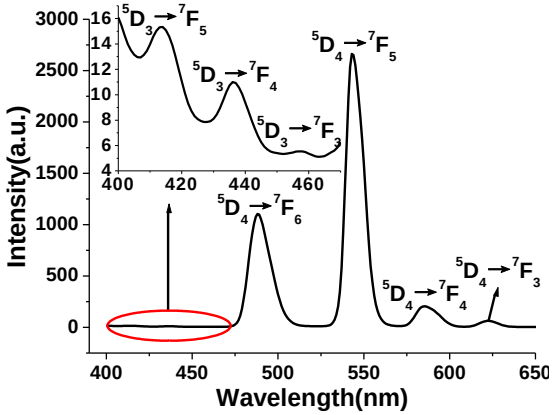

Fig. 6. The emission spectrum of glass $Ca_{1\text{-}0.0625}AlB:Tb^{3+}{}_{0.0625}$ under 378 nm excitation.

According the excitation spectrum of Tb^{3+} ion, this high calcium aluminoborate glass with the simple composition of $CaO\text{-}Al_2O_3\text{-}B_2O_3\text{-}Tb_2O_3$ could been excited both by near ultraviolet LED diode (wavelength region 380 nm～400 nm) and by blue LED diode (wavelength region 450 nm～475 nm), emiting strong green luminescence.

3.3 Concentration-dependent luminescence of Tb^{3+} in glass CaAlB:Tb^{3+}

Fig. 7A shows the variation of green emission intensity ($^5D_4 \rightarrow {}^7F_5$) at 544 nm as a function of Tb^{3+} concentration (x) in glass with the composition of $Ca_{1-x}AlB:Tb^{3+}{}_x$ under 378 nm (curve a) and 486 nm (curve b) excitation, and Fig. 7B shows the variation of purple emission intensity ($^5D_3 \rightarrow {}^7F_5$) at 414 nm as a function of Tb^{3+} concentration (x) excited by 378 nm (curve c). It is clear that the $^5D_4 \rightarrow {}^7F_5$ emission is much more intense than $^5D_3 \rightarrow {}^7F_5$ emission. When excited by 378 nm, the green emission (544 nm) intensities ($^5D_4 \rightarrow {}^7F_5$) of Tb^{3+} ions (curve a in Fig. 7A) increase with the enhancive concentrations of Tb^{3+} in glasses up to 15.6 mol% and then keep unchangeably up to 21.9 mol% as a result of concentration quenching. On the other hand, when excited by 486 nm (curve b in Fig. 7A), the emission intensities of Tb^{3+} at 544 nm increase almost proportionally to the Tb^{3+} concentrations up to 21.9 mol% without prominent concentration quenching phenomenon. In Fig. 7B, the purple emission intensities ($^5D_3 \rightarrow {}^7F_5$) of Tb^{3+} ions at 414 nm decrease with the increase of Tb^{3+} concentrations in glasses. This phenomenon was reported in most of Tb^{3+}-doped silicate glasses [7,11], and the non-radiative processes such as multi-phonon decay, quenching by impurities and energy migration among active ions are mainly responsible for the quenching of dopant luminescence efficiency.

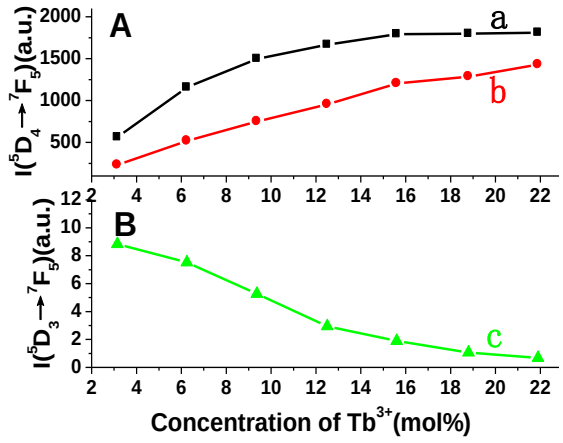

Fig. 7. Variation of green ($^5D_4$-$^7F_5$) and purple ($^5D_3$-$^7F_5$) emission intensities of Tb^{3+} as a function of Tb^{3+} concentration (mol%) in $Ca_{1-x}AlB:Tb^{3+}{}_x$ under 378 nm (curve a,c) and 486 nm(curve b) excitation.

The variation of relative intensities ratio of excitation peaks (I_{486}/I_{378}) due to transitions $^7F_6 \rightarrow {}^5D_4$ (486 nm) and $^7F_6 \rightarrow {}^5D_3$ (378 nm) as a function of Tb^{3+} concentrations in glasses $Ca_{1-x}AlB:Tb^{3+}{}_x$ has been presented in Fig. 8. The curve showed the ratios (I_{486}/I_{378}) enhances with the increase of Tb^{3+} concentration, confirming the fact that the multi-phonon assisted non-radiative relaxation transfer of $^5D_3 \rightarrow {}^5D_4$ increases with the enhance of Tb^{3+} concentration, resulting in the enhancive populations on $^5D_4$ energy level and the reduced populations on $^5D_3$ energy level. Consequently, it is advantageous to high Tb^{3+} concentration glass excited with blue-light wavelength.

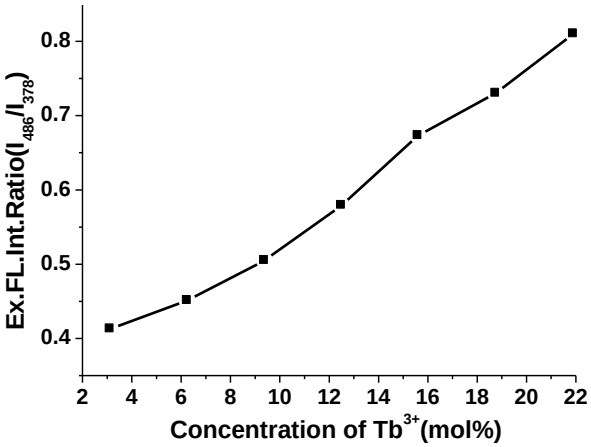

Fig. 8. Variation of relative excitation fluorescence intensity ratio (I_{486}/I_{378}) as a function of Tb^{3+} concentrations in glasses $Ca_{1-x}AlB:Tb^{3+}{}_x$.

Atul D. Sontakke et al [7] has proved that in aluminosilicate glass host, since the highest lattice phonon energy is found to be around 1030 cm^{-1}, the multi-phonon decay can be neglected. At low Tb^{3+} concentrations, there is a high possibility of multi-phonon assisted non-radiative relaxation of $^5D_3$ to $^5D_4$ levels due to its low energy gap around 5990 cm^{-1}, but at higher concentrations, this could be dominated by a faster cross-relaxation (CR) phenomenon due to a resonance energy transfer (RET) through $^5D_3 \rightarrow {}^5D_4 \Rightarrow {}^7F_6 \rightarrow {}^7F_0$ process as the energy difference between $^5D_3$ and $^5D_4$ matches well with the energy gap between $^7F_6$ and $^7F_0$ energy levels [29]. But in the present aluminoborate glass system the multi-phonon assisted non-radiative relaxations from $^5D_3$ to $^5D_4$ level are also very much expected due to the higher energy phonons (~1300 cm^{-1}) of B—O bonds in the host matrix [28]. According the energy level diagram of Tb^{3+} ion in Fig. 9, when excited by 378 nm ($^7F_6 \rightarrow {}^5D_3$), the excited electrons at $^5D_3$ energy level relax to $^5D_4$ energy level by multi-phonon assisted non-radiative energy transfer, inducing the decrease of $^5D_3 \rightarrow {}^7F_5$ transitions and the increase of $^5D_4 \rightarrow {}^7F_5$ transitions. When the Tb^{3+} concentration is over 15.6 mol%, the cross relaxation processes through $^5D_3 \rightarrow {}^5D_4 \Rightarrow {}^7F_6 \rightarrow {}^7F_0$ become more prominent, inducing concentration quenching phenomenon [7]. But under 486 nm excitation, the multi-phonon assisted non-radiative transfer of $^5D_3 \rightarrow {}^5D_4$ and the cross relaxation energy transfer through $^5D_3 \rightarrow {}^5D_4 \Rightarrow {}^7F_6 \rightarrow {}^7F_0$ process disappear simultaneously [7], only energy migration among excited state active ions is the possible route to transfer energy, so the emission of $^5D_4 \rightarrow {}^7F_5$

transitions increase almost proportionally up to 21.9 mol% of Tb^{3+} concentration without concentration quenching phenomenon.

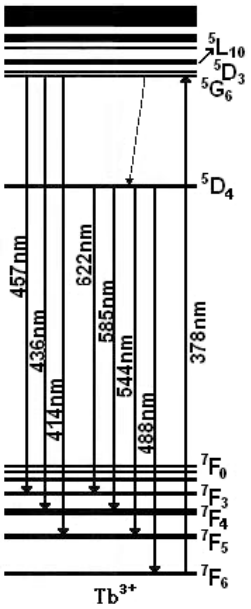

Fig. 9. Partial energy level diagram of Tb^{3+}.

Consequently, in this calcium aluminoborate glass, under 378 nm excitation, the optimum Tb^{3+} concentration is 15.6 mol% (equal to 17.2 wt% Tb_2O_3 in glass CaAlB:Tb^{3+}), but under 486 nm excitation, the concentration quenching processes were very weak when Tb^{3+} concentration is up to 21.9 mol% (22.7 wt% Tb_2O_3 in glass). This is a high quenching concentration of Tb^{3+} for glass hosts. Similar result was also reported by Yamashita et al [2] in borosilicate glasses ($60.8SiO_2$–$10.1B_2O_3$–$14.5Na_2O$–$5.1Al_2O_3$–$5.7CaO$–$3.8ZrO_2$). So this CaO-Al_2O_3-B_2O_3 glass matrix has a fine ability of molting rare earth oxides at relative low temperature (1200 ℃) comparison with silicate glass matrix.

3.4 CIE chromatic coordinates of glass CaAlB:Tb^{3+}

According to Z.D. Lou et al's article [30], the chromatic coordinates, dominant wavelengths and color purity values of glass samples compared to 1931 CIE Standard Source C [illuminant C = (0.3101, 0.3162)] are determined from the emission spectra of Tb^{3+} excited by 378 nm wavelength and the results are listed in Table 1 and represented in Fig. 10. The glasses emit green light with slight yellow (points a and b) under 378 nm excitation and yellowish green light (point c) with 485 nm excitation. Consequently, the luminescence emission color of glasses change with the excitation wavelength, but relatively stabilize with Tb^{3+} concentration.

Table 1. Chromatic coordinates, dominant wavelengths and color purity values for as-prepared glass samples under 378 nm excitation.

Samples	CIE(x,y)	Dominant wavelength(nm)	Color purity (%)
CaAlB:$Tb^{3+}_{0.0313}$(point a)	0.252,0.576	537.0	58.2
CaAlB:$Tb^{3+}_{0.0625}$	0.256,0.591	539.0	61.4
CaAlB:$Tb^{3+}_{0.0938}$	0.258,0.598	540.0	63.8
CaAlB:$Tb^{3+}_{0.156}$	0.260,0.599	540.5	64.0
CaAlB:$Tb^{3+}_{0.219}$(point b)	0.261,0.603	541.0	66.4

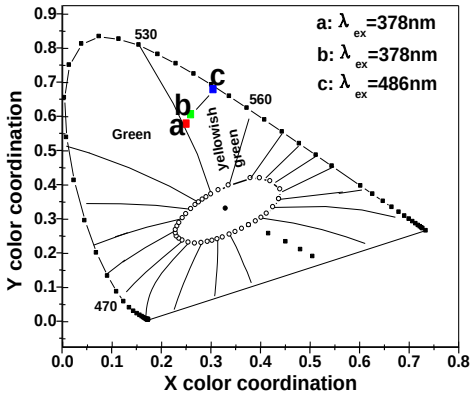

Fig. 10. CIE1931 chromaticity diagram showing the chromaticity points of glasses $Ca_{1-x}AlB:Tb^{3+}_x$ with Tb^{3+} concentrations and excitation wavelengths.

3.5 Effect of Si^{4+} concentration on luminescence of Tb^{3+}

Fig. 11 shows the variation of green emission (544 nm) intensity of Tb^{3+} in glass with composition of $(Ca_{1-0.125-y}Si_y)AlB:Tb^{3+}_{0.125}$ as a function of Si^{4+} concentration (mol%) under 378 nm excitation. The emission intensities raise obviously with the increase of Si^{4+} concentrations up to 12.5 mol% (equal to 4.74 wt% SiO_2 in glass) and decrease subsequently. When a small quantity of SiO_2 is integrated in glass, the form of $[SiO_4]$ structure unit improves the stability of glass skeleton structure, decreases the thermal expansion coefficient of glass matrix [31], and enhances the emission intensity of Tb^{3+} [32]. With the increase of SiO_2 concentrations farther, the sintering temperature of glass will arise. If keeping sintering at 1200 ℃, the glasses could not been melted totally and become opacity and uneven, resulting in low emission intensity of Tb^{3+} in glass.

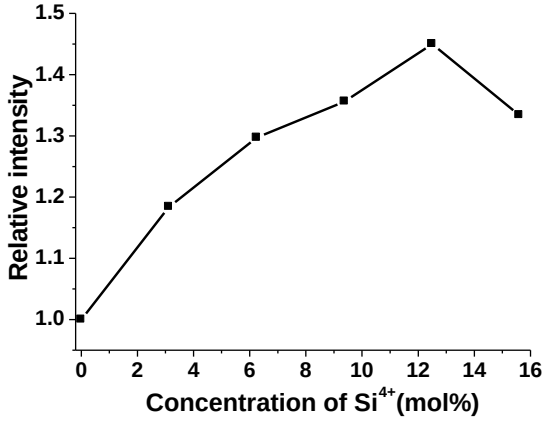

Fig. 11. Emission intensities (544 nm) of Tb^{3+} in glasses $(Ca_{1-0.125-y}Si_y)AlB:Tb^{3+}_{0.125}$ as a function of Si^{4+} concentration (mol%) under 378 nm excitation.

3.6 Effect of Li^+ concentration on luminescence of Tb^{3+}

When a trivalent metallic ion, such as Tb^{3+}, is incorporated into a host lattice and substitutes a divalent metallic ion site (like Ca^{2+}), an extra positive charge generates to the lattice. This extra positive charge can be compensated by the incorporation of monovalent ion, like Li^+ ion [33]. Fig. 12 shows the variation of green emission (544 nm) intensity of Tb^{3+} in glass with the composition of $(Ca_{1-0.125-z/2}Li_z)AlB:Tb^{3+}_{0.125}$ as a function of Li^+ concentration (mol%) under 378 nm exctiation. The luminescence of Tb^{3+} enhances about 1.4 fold when the concentration of Li^+ is up to 12.5 mol% (equal to 0.60 wt% Li_2O in glass), then decreases evidently. Lithium ion is small enough to inhabit any crystal lattice position, like Ca^{2+} ion or interspace site in lattice. According to the compensated principle, the total compensated concentration of Li^+ is 12.5 mol%. Under this concentration, Li^+ ions act as charge compensation ions for Tb^{3+} in the lattice [34], so the emission intensities of Tb^{3+} enhance with the increase of Li^+ concentration. When the molarity of Li^+ ion exceeds 12.5 mol%, the superfluous Li^+ ions probably occupy Ca^{2+} sites in the lattices, generate extra negative charges which is speculated to generate oxygen vacancies for charge neutrality, resulting in the weakening of glass stability and the decrease of luminescence of Tb^{3+} [35].

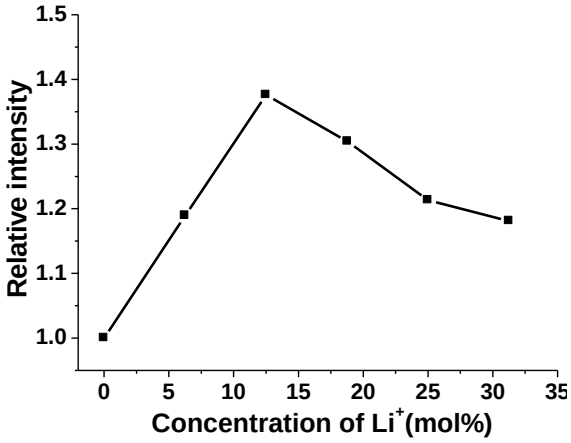

Fig. 12. Emission intensities (544 nm) of Tb^{3+} in glasses $(Ca_{1-0.125-z/2}Li_z)AlB:Tb^{3+}_{0.125}$ as a function of Li^+ concentration (mol%) under 378 nm excitation.

On the other hand, the doping Li_2CO_3 reagent in glass raw materials plays a role as fluxing agent [36], resulting in the fall in glass melting temperature. Synchronously, Li^+ ion easily inserts into glass lattices to relax the strain, inducing the decrease of glass viscosity in molten state which make molding process easy [35].

4. Conclusions

The new calcium aluminoborate glass matrix with the composition of CaO-Al_2O_3-B_2O_3 has been prepared by melting at 1200 ℃ for 3 h in air. This glass matrix possesses high glass transition temperature, good transmittance, low synthesis temperature and good thermal stability. The Tb^{3+}-doped glasses have strong green emission at 544 nm and the optimum concentration of Tb^{3+} is 15.6 mol% under 378 nm excitation. When excited by 486 nm, the effect of concentration quenching process on Tb^{3+} luminescence was very weak when Tb^{3+} concentrations increase up to 21.9 mol%. Obvious, the increase of Tb^{3+} emission intensity in this glass can be achieved through doping small quantities of Li_2O or SiO_2 in glass. Meanwhile, the presence of SiO_2 can improve the stability of lattice structure, and the incorporation of Li_2O can reduce glass viscosity in molten state.

Acknowledgments

This project is financially funded by both the Foundation of Chinese Overseas Returned Personnel (2006-331) and Nano-Project of Guangzhou City, People's Republic of China (2007Z3-D2041).

References

[1] X. Y. Sun, S. M. Huang, M. Gu, Q. C. Gao, X. S. Gong, Z. P. Ye, Physica B **405**, 569 (2010).
[2] T. Yamashita, Y. Ohishi, J. Non-Cryst. Solids **354**, 1883 (2008).
[3] W. Liu, D. P. Chen, T. Akai, Mater. Chem. Phys. **109**, 257 (2008).
[4] L. H. Huang, X. J. Wang, H. Lin, X. R. Liu, J. Alloys Compd. **316**, 256 (2001).
[5] H. Lin, E. Y. B. Pun, X. J. Wang, X. R. Liu, J. Alloys Compd. **390**, 197 (2005).
[6] Z. Pan, K. James, Y. Cui, A. Burger, N. Cherepy, S. A. Payne, R. Mu, S. H. Morgan, Nucl. Instrum. Methods Phys. Res., Sect. A **594**, 215 (2008).
[7] A. D. Sontakke, K. Biswas, K. Annapurna, J. Lumin. **129**, 1347 (2009).
[8] L. H. Huang, W. X. Chen, Y. L. Liu, J. Funct. Mater.(Chinese) **37**, 861 (2006).
[9] D. M. Krol, R. P. van Stapele, J. H. Haanstra, T. J. A. Popma, G. E. Thomas, A. T. Vink. J. Lumin. **37**, 293 (1987).
[10] A. J. Silversmitha, D. M. Boye, K. S. Brewer, C. E. Gillespie, Y. Lu, D. L. Campbell, J. Lumin. **121**, 14 (2006).
[11] D. M. Boye, A. J. Silversmith, T. N. Nguyen, K. R. Hoffman, J. Non-Cryst. Solids **353**, 2350 (2007).
[12] G. R. Chen, Y. X. Yang, D. H. Zhao, F. Xia, J. Am. Ceram. Soc. **88**, 293 (2005).
[13] C. H. Kam, S. Buddhudu, Physica B **337**, 237 (2003).
[14] P. Fabeni, G. P. Pazzi, M. Martini, A. Vedda, M. Nikl, K. Nitsch, S. Baccaro, Radiat. Meas. **33**, 721 (2001).
[15] S. Baccaro, A. Cecilia, M. Montecchi, M. Nikl, P. Polato, G. Zanella, R. Zannoni, J. Non-Cryst. Solids **315**, 271 (2003).
[16] H. N. Sooraj, R. Y. Prabhakara, S. Buddhudu, Mater. Lett. **48**, 303 (2001).
[17] J. E. Shelby, J. Am. Ceram. Soc. **66**, 225 (1983).
[18] A. Kazuo, N. Hiroshi, K. Ken, H. Tatsutoku, I. Yoshiro, H. Takashi, J. Appl. Phys. **59**, 3430 (1986).
[19] F. R. Zeng, R. F. Gao, Z. Q. Mao, H. O. Qiu, Chin. J. Inorg. Chem. **24**, 808 (2008).
[20] H. C. Yi, J. Y. Guigne, L. A. Whalen, J. J. Moore, J. Mater. Synth. Process. **8**, 15 (2000).
[21] J. Li, S. P. Xia, S. Y Gao, Spectrochim. Acta Part A **51**, 519 (1995).
[22] C. M. B. Henderson, D. Taylor, Spectrochim. Acta, Part A: Mol. Spectrosc. **35**, 929 (1979).
[23] A. S. Tenney, J. Wong, J. Chem. Phys. **56**, 5516 (1972).
[24] Y. Z. Jia, Y. Zhou, S. Y. Gao, Chin. J. Inorg. Chem.(Chinese) **17**, 636 (2001).
[25] P. N. Huang, X. H. Huang, Acta Optica. Sinica.(Chinese) **7**, 524 (1987).
[26] V. P. Klyuev, B. Z. Pevzner, Glass Phys. Chem. **29**, 127 (2003).
[27] T. Tsuboi, Eur. Phys. J. Appl. Phys. **25**, 95 (2004).
[28] K. Annapurna, R. N. Dwivedi, P. Kundu, S. Buddhudu, J. Mater. Sci. **40**, 1051 (2005).
[29] Y. C Yoon, K. S. Sohn, H. D. Park, S. Y. Choi, J. Mater. Res. **16**, 881 (2001).
[30] Z. D. Lou, J. H. Hao, Thin Solid Films **450**, 334 (2004).
[31] L. Peng, G. L. Zhao, H. Ying, J. X. Wang, W. J. Weng, G. R. Han, J. Chin. Ceram. Soc. **35**, 856 (2007).
[32] C. Bueno, R. A. Buchanan, Glass(Ⅱ) **1327**, 79 (1990).
[33] P. V. Kelsey, Jr., J. J. Brown, Jr., J. Electrochem. Soc. **123**, 1384 (1976).
[34] L. H. Tian, S. I. Mho, Solid State Commun. **125**, 647 (2003).
[35] L. D. Sun, C. Qian, C. S. Liao, X. Wang, C. H. Yan, Solid State Commun. **119**, 393 (2001).
[36] L. P. Lu, X. Y. Zhang, Z. H. Bai, X. C. Wang, X. Y. Mi, Q. S. Liu, Adv. Powder Technol. **17**, 181 (2006).

* Corresponding author: tiesl@scnu.edu.cn